Inorganic Chemistry

Article

pubs.acs.org/IC

Triangular Exchange Interaction Patterns in $K_3Fe_6F_{19}$: An Iron Potassium Fluoride with a Complex Tungsten Bronze Related Structure

Francesco Mezzadri,*[,†,⊥] Gianluca Calestani,[†,‡] Lara Righi,[†] Chiara Pernechele,[§] Massimo Solzi,[§] and Clemens Ritter[∥]

[†]Dipartimento di Chimica, Università di Parma, Parco Area delle Scienze 17/A, 43124 Parma, Italy

[‡]IMEM-CNR, Parco Area delle Scienze 37/A, 43124 Parma, Italy

[§]Dipartimento di Fisica e Scienze della Terra, Università di Parma, Parco Area delle Scienze 7/A, 43124 Parma, Italy

[∥]Institute Laue-Langevin, Boite Postale 156, F-38042, Grenoble, France

Supporting Information

ABSTRACT: The synthesis and structural and magnetic characterizations of $K_3Fe_6F_{19}$, a new iron potassium fluoride with a complex tungsten bronze related structure, are presented. This phase was found during the investigation of relatively low-temperature (600 °C) synthesis conditions of classical tetragonal tungsten bronze (TTB) fluorides and can be considered an intermediate that forms at this temperature owing to faster crystallization kinetics. The $K_3Fe_6F_{19}$ compound has an orthorhombic structure (space group *Cmcm* (63), a = 7.6975(3) Å, b = 18.2843(7) Å, c = 22.0603(9) Å) related to the TTB one, where the perovskite cage is substituted by a large S-shaped channel simultaneously occupied by two potassium atoms. The magnetic structure, characterized by magnetization measurements on an oriented single crystal and powder neutron diffraction, is dominated by the presence of interconnected double stripes of antiferromagnetic triangular exchange interaction patterns alternately rotated in clock- and anticlockwise fashion. The magnetic order takes place in a wide temperature range, by increasing progressively the interaction dimensionality.

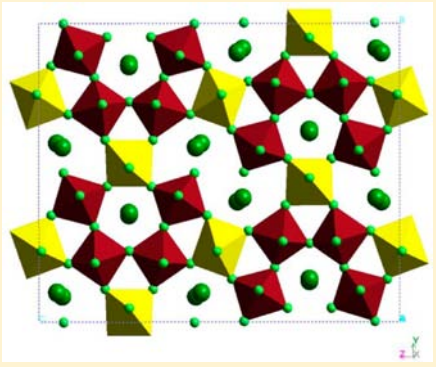

INTRODUCTION

Multiferroic fluorides with a tetragonal tungsten bronze (TTB) structure, having the formula $K_{2+x}Fe_5F_{15}$ ($0 \le x \le 1$),[1−3] are characterized by peculiar spin structures where the presence of triangular exchange interaction patterns (typical of kagome lattices) gives rise to ferrimagnetism as a consequence of magnetic frustration. Their complex magnetic behavior remained for a long time not completely understood, and just very recently, it has been clarified for the potassium-rich end-member ($K_3Fe_5F_{15}$) by combining the information obtained by magnetization measurements carried out on oriented crystals, Mössbauer spectroscopy, and powder neutron diffraction data.[4] During some attempts to synthesize TTB fluorides at relatively low temperature (600 °C), aiming to better define their preparative conditions, the presence of a new phase giving a complex XRD pattern was observed. The phase, present in the sample as the majority product together with small amounts of $KFeF_4$ and TTB phases, was found to disappear, transforming into the TTB one, by a further treatment at the temperatures (700−800 °C) that are usually used for its synthesis. The phase was, therefore, considered as an intermediate that forms at lower temperatures because of a faster crystallization kinetics. The crystal structure and chemical composition were determined by single-crystal XRD analysis. The phase, which resulted to having a $K_3Fe_6F_{19}$ composition, has an orthorhombic structure (space group *Cmcm* (63), a = 7.6975(3) Å, b = 18.2843(7) Å, c = 22.0603(9) Å) related to the TTB one, showing S-shaped channels along the x direction, formed by eight FeF_6 octahedra. These peculiar rings are obtained as a distortion of the "classical" TTB framework, in addition to triangular and pentagonal cationic sites. In analogy with the multiferroic $K_3Fe_5F_{15}$ compound,[5] both charge ordering involving Fe^{2+}/Fe^{3+} ions and FeF_6 octahedra tilting are detected, but polar properties are prevented by the centrosymmetric nature of the structure. Among fluorides with a TTB assembly, the present compound represents a new case showing peculiar structural and magnetic features. Several materials indeed are known having a TTB-derived structure, for example, tetragonal,[6] orthorhombic,[7] or hexagonal[8] tungsten bronzes, while pyrochlores show different structures and a similar stoichiometry.[9] However, the presence of these large S-shaped cavities, occupied simultaneously by two potassium ions per layer, makes this system quite interesting for its structural features involving unusual coordination numbers and geometries.[10] At the same time, this compound exhibits unconven-

Received: July 8, 2013
Published: October 15, 2013

   dx.doi.org/10.1021/ic401749q | *Inorg. Chem.* 2013, 52, 12599−12604

tional magnetic properties related to the magnetic ordering involving interconnected double stripes of triangular exchange interaction patterns. For all of these reasons, the new form showing the $K_3Fe_6F_{19}$ composition was isolated by adjusting the starting stoichiometry and the complete magnetic and structural characterization was undertaken.

EXPERIMENTAL SECTION

In a typical procedure, a silver tube was filled with a stoichiometric mixture of KF, FeF_2, and FeF_3 and mechanically sealed. The tube was then heat-treated at 550−650 °C for 12 h in a nitrogen atmosphere and finally cooled down to room temperature. In these conditions, the reaction product is usually well-crystallized and single crystals suitable for XRD experiments and magnetic measurements can be extracted from the reacted mass. Polycrystalline samples were characterized by powder X-ray diffraction (PXRD) by using a Thermo ARL X'tra diffractometer, equipped with Cu Kα radiation and a Si(Li) Thermo Electron solid state detector in order to eliminate the fluorescence contribution of iron. Diffraction patterns were collected in the 10−70° 2θ range, with 0.02° steps and counting times of 2 s. Temperature-dependent diffraction experiments were performed by using an Anton Paar TTK450 chamber in the temperature range of 80−700 K. Single-crystal XRD experiments were carried out by using a Bruker APEX II diffractometer equipped with a CCD area detector and graphite monochromatized Mo Kα radiation. Structure solution and refinement were carried out using the Sir2004[11] and Shelx97[12] programs, respectively. The magnetic characterization was performed by means of a SQuID magnetometer (MPMS XL5 Quantum Design, maximum applied field 5 T) in the temperature range of 5−300 K. In particular, zero field cooling (ZFC) and field cooling (FC), both in cooling (FCC) and in warming (FCW) curves, were measured in an applied field of H_a = 50 Oe on powder samples. $M(T)$ curves were measured on cooling and heating in an applied field of 5000 Oe along different crystallographic axes in the cases of the single-crystal sample and powder samples. Neutron powder diffraction (NPD) data were collected every 5° in the temperature range of 5−300 K with the high-intensity powder diffractometer D20 (λ = 2.39 Å) at the Institute Laue-Langevin (ILL), Grenoble, France. Additional high-resolution data (λ = 2.39 Å, step = 0.05°) were taken at T = 2, 70, 100, 150, and 300 K on the high-resolution powder diffractometer D2B, situated as well at the ILL. All the refinements were carried out using the GSAS package.[13,14]

RESULTS AND DISCUSSION

Nuclear Structure Determination. The crystal structure of $K_3Fe_6F_{19}$ was determined by single-crystal X-ray diffraction through the collection of 2475 reflections in the 0−60° 2θ range. The symmetry is orthorhombic, space group *Cmcm* (63), with a = 7.6975(3) Å, b = 18.2843(7) Å, and c = 22.0603(9) Å. The structure was full-matrix refined using 150 parameters, yielding agreement factors R_1 = 0.0504, wR_2 = 0.0814, and GOF = 0.994. No substantial deviation from the expected stoichiometry was suggested by the refinement of the site occupation factors so that, in the final cycles, all the atomic positions were refined with full occupancy.

Crystal data and refined atomic parameters and selected bond distances are reported as Supporting Information in Tables S1−S2. The structure, whose projection on the *bc* plane is shown in Figure 1, presents structural building blocks similar to those characterizing the TTB lattice. However, the presence of an additional octahedral FeF_6 unit, with respect to $K_3Fe_5F_{15}$, produces a different assembling in which only triangular and pentagonal cavities are retained, whereas the perovskite cage is substituted by a larger S-shaped one, simultaneously occupied by two potassium ions. A comparison of the two structures is reported in Figure 2, where the fundamental structural block

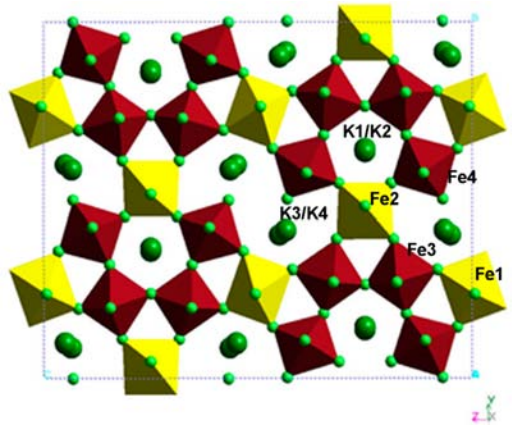

Figure 1. Crystal structure of $K_3Fe_6F_{19}$ projected onto the *bc* plane. Dark green spheres represent the potassium ions, light green indicates fluorine, while dark red and yellow octahedra are occupied by Fe(III) and Fe(II), respectively. K1, K3 and K2, K4 atoms lie on the mirror plane at x = 0 and x = 1/2, respectively.

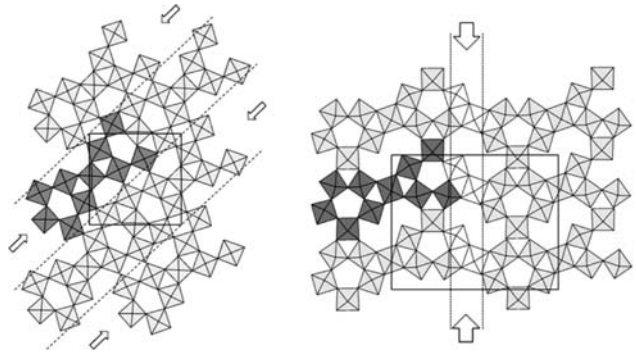

Figure 2. Comparison of the crystal structures of $K_3Fe_6F_{19}$ (left) and $K_3Fe_5F_{15}$ (right). The common structural blocks are represented in dark gray, evidencing the different stacking schemes in the two compounds; the insertion of the additional FeF_6 octahedra, leading to the $K_3Fe_6F_{19}$ stoichiometry, is pointed out in the right panel by vertical arrows.

shared by the two models is highlighted. The basic difference consists of the stacking sequence of these blocks, which are slightly shifted with respect to the $K_3Fe_5F_{15}$ arrangement, with the consequent suppression of the square, perovskite-like cationic site and the creation of the S-shaped cavity. Two similar layers of FeF_6 vertex-sharing polyhedra are stacked along the x direction in the unit cell; in analogy with the well-known TTB potassium iron fluorides, the doubling of the stacking sequence is related to a cooperative tilt of the octahedral units with respect to the stacking axis, producing a displacement of the apical fluorine ions in the *bc* plane. The analysis of the Fe−F bond distances, reported in Table S2 (Supporting Information), reveals the existence of charge ordering induced by the presence of iron(II) and (III) in the structure. Within this picture, Fe1 and Fe2 result to being divalent iron sites, while Fe3 and Fe4 are occupied by trivalent iron ions, giving the formula $K_3Fe^{II}_2Fe^{III}_4F_{19}$, which complies with the stoichiometry requirements. An unusual coordination of the potassium ions is detected for the K3 and K4 sites in the large cavity, showing a quite distorted array of bonds, with K−F distances ranging from 2.564 to 3.158 Å.

Magnetic Characterization. Magnetic measurements performed in the temperature range of 5−300 K on a powder

dx.doi.org/10.1021/ic401749q | Inorg. Chem. 2013, 52, 12599−12604

sample show a complex field-dependent behavior characterized by a series of critical effects. As far as low fields are applied (Figure 3a), that is, H_a = 50 Oe, the ZFC and FC curves result

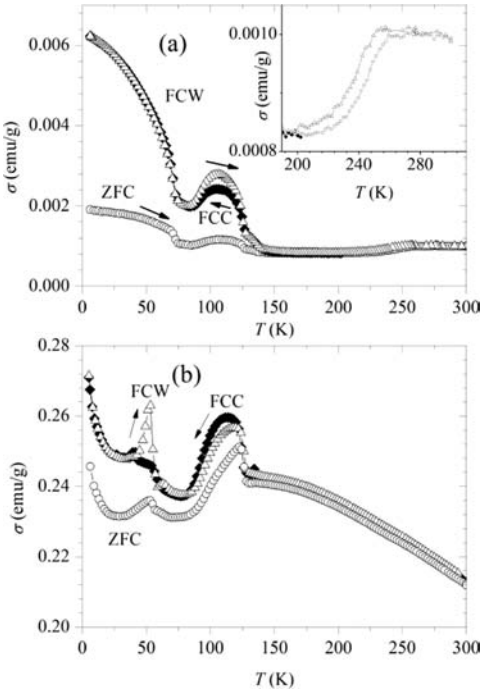

Figure 3. Magnetization measurements of a powder sample. (a) The applied field is 50 Oe, and FCC and FCW indicate field cooling measurements performed on cooling and warming, respectively. In the inset, a zoom of the observed anomaly at 260 K is displayed. (b) ZFC FCC and FCW curves, measured for an applied field of 5000 Oe; the arrows indicate warming or cooling direction.

to being superimposed in the range of 150−300 K, and a small anomaly at about 260 K is pointed out. A first significant increase of the magnetization (clearly evident in FC curves) occurs at 150 K, followed by a second and sharper increase at 125 K, leading to a maximum around 110 K.

A further effect is observed at about 70 K, where an increase of the measured magnetization is observed while reducing the temperature, clearly evident in both FC and ZFC curves. The behavior displayed with higher applied fields (H_a = 5000 Oe) is quite different (Figure 3b), with the disappearance of the anomalies observed at 260 K (which is, however, evidenced by the inverse susceptibility curve as a switch from linear to parabolic regime) and 150 K. On the contrary, the transition at 125 K is still present and the sharp increase at 70 K appears to be slightly shifted to a lower temperature (about 60 K), assuming at the same time the typical features of an AFM transition (as confirmed by the magnetic structure deduced from neutrons, discussed in detail in the next paragraph). The observed difference between low- and high-field measurements on this transition can be attributed to the field effect on a "canted" (or more generally "frustrated") AFM structure. However, a discrepancy exists also in field cooling curves recorded on cooling or warming, magnified in the high-field measurements (Figure 3b). While the system is heated from 5 K (ZFC and FCW curves), the first transition assumes the typical feature of an AFM character before undergoing the 125 K transformation. On the contrary, when the system is cooled down (FCC) after having ordered its moments at 125 K, the further transition is less evident and appears as a large and smoothed peak. More detailed information was obtained performing the measurements on an oriented single crystal, with the magnetic field applied along the three fundamental crystallographic directions. Owing to the reduced crystal mass (0.48 mg) and to the limited magnetic response, the measurements carried out at 50 Oe resulted to being quite scattered so that they were repeated, increasing the applied magnetic field to 5000 Oe. Because the behavior is qualitatively similar, only the high-field measurements are here reported (Figure 4). The measurements performed with the field applied

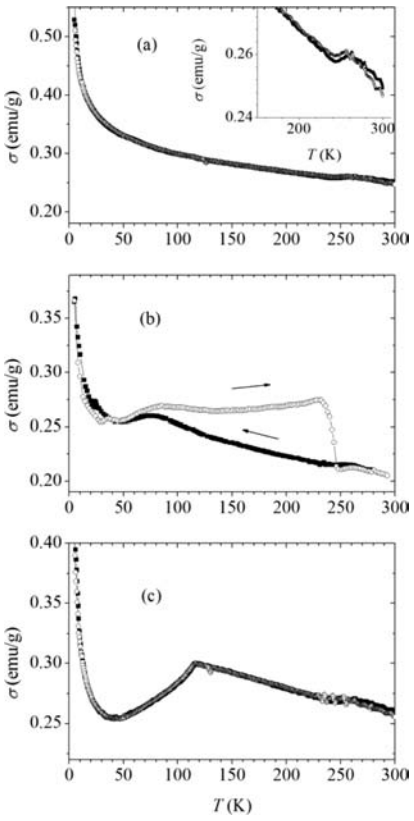

Figure 4. ZFC (open symbols) and FC (full symbols) magnetization measurements on a single crystal with the field applied of 5000 Oe along the *a* axis (panel a), *b* axis (panel b), and *c* axis (panel c). In the inset of panel a, the details of the anomaly observed at 260 K are reported. The arrows, where present, indicate heating or cooling measurements.

along *a* (Figure 4a) reveal a very weak effect at 260 K, evidenced in the inset of Figure 4a, suggesting that the ordering phenomena do not develop a relevant component of the magnetic moments along this axis.

The weak anomaly at 260 K is observed also in the measurements with the field applied along *c* (Figure 4c), where a clear antiferromagnetic (AFM) transition takes place at 125 K. Different from the others, the measurements along *b* (Figure 4b) strongly depend on the heating/cooling procedure. On one side, on cooling, the 260 K anomaly is followed by an AFM transition at about 70 K. On the other side, on heating, not only the magnetization does not decrease significantly above the transition (shifted to a slightly higher temperature) but also it increases slowly above 125 K so that the 260 K anomaly is preceded by a ferromagnetic-like transition at 245 K. The picture emerging from the comparison of powder and single-

dx.doi.org/10.1021/ic401749q | *Inorg. Chem.* 2013, 52, 12599−12604

crystal measurements is quite complex. Indeed, the three main transitions observed on the powder sample are clearly evidenced on a single crystal and reveal a globally AFM nature of the system. However, whereas the 260 K transition shows an isotropic behavior, the remaining two magnetic interactions exhibit a clear anisotropic character and are triggered only when the field is applied alongside the proper crystallographic direction (b and c for the 80 and 125 K transitions, respectively). Conversely, the transition taking place at 150 K is not sufficiently evidenced by single-crystal measurements, and therefore, it is not possible to clarify its nature on the basis of the performed magnetic characterization. It has to be noted that both the powder and the crystal samples' mass magnetizations are positive and far from the zero value at room temperature in both low and high magnetic fields. We suppose, in analogy to what was observed for $K_3Fe_5F_{15}$, that this is due to a Van Vleck paramagnetic signal almost independent from temperature.[4]

Magnetic Structure by Neutron Diffraction. The evolution of the magnetic structure as a function of the temperature was studied by powder neutron diffraction data collected at temperatures ranging from 5 to 150 K. The analysis of the magnetic contribution to the diffraction patterns revealed a complex behavior resumed in Figure 5, on the basis of which

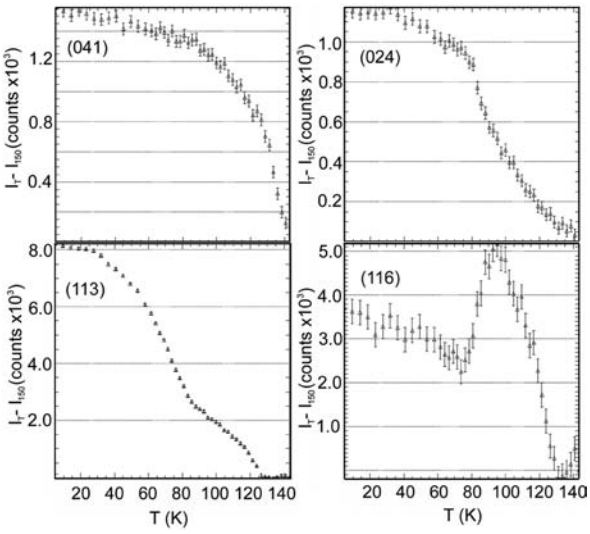

Figure 5. Neutron diffraction intensities of the (041), (024), (113), and (116) reflections normalized with respect to the value observed at 150 K.

the reflections can be grouped in three fundamental classes. The first class groups reflections showing a magnetic contribution to the diffracted intensity starting below 150 K, well above the 125 K AFM transition. Although the complexity of the diffraction pattern and the limited intensity of the magnetic peaks at these temperatures prevent the unambiguous attribution of the reflections, the analysis suggests that this class includes only $0kl$ reflections ($h = 0$). In this hypothesis, the anomaly observed in the $M(T)$ curves at about 260 K would be related to the establishment of a short-range ordering of AFM interactions that acquires a pronounced two-dimensional (2D) character (involving the bc plane) below 150 K. This behavior would find some analogies in $KFeF_4$, which is reported to show 2D magnetic order at room temperature, with the onset of 3D order below 137 K.[15,16] In our case, the 3D ordering would take place below 125 K, where all the remaining reflections show magnetic contributions. The second class includes reflections that, after a first increase of the magnetic intensity below 125 K, undergo a second strong enhancement starting from 80 K (for example, the (113) reflection shown in Figure 5).

For the third class, the magnetic intensity, after a maximum at 100 K, decreases until 80 K, where it starts again to rise smoothly as in the case of the (116) reflection in Figure 5. The temperature dependence of the magnetic intensities of the last two series of reflection classes suggests 80 K as an important temperature for the evolution of the magnetic structure. This hypothesis is confirmed also by the intensity trend of some $0kl$ reflections, like the case of the (024) reflection in Figure 5, for which a change is as well already observed at this temperature. The refinement of the collected data was carried out in the colored space group *Cmcm*, with no time-inversion symmetry operators. Two additional phases, namely, $KFeF_4$ and $K_{2.5}Fe_5F_{15}$, were included as secondary phases in the refinement. The x components (M_x) of the atomic moments, converging to negligible values in the preliminary steps of the refinement, were constrained to zero for all the iron atoms in the whole temperature range investigated.

The refined magnitude of the atomic moment for the four independent iron sites is reported in Figure 6 as a function of

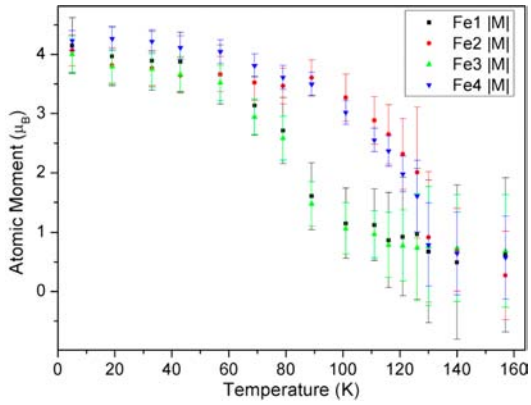

Figure 6. Temperature dependence of the atomic moments.

the temperature, pointing out a different behavior for Fe2 and Fe4 on one side and Fe1 and Fe3 on the other. By decreasing T, the moments of the former atoms increase suddenly at 125 K, whereas those of the latter ones, at first gradually increasing, rise up at 80 K, giving an intuitive justification of the effects observed at these temperatures in the trend of the diffracted intensities. The magnitude of all the atomic moments becomes then comparable below 60 K. While the Fe2 and Fe4 moments are directed along the c axis in the whole temperature range, those of Fe1 and Fe3, as shown in Figure 7, undergo a rotation by decreasing the temperature, giving rise to a smooth transition between two different magnetic structures that extends on a wide temperature range and is reflected in the smoothed behavior of the magnetization recorded on cooling. At 100 K, just below the AFM transition taking place at 125 K, the Fe2 and Fe4 moments, oriented in the c direction and possessing a significant modulus, are AFM ordered in the bc plane, as shown in Figure 8. The situation of Fe1 and Fe3, which form chains of vertex-sharing octahedra running along c, is more difficult to define accurately at this temperature, because of the small values of their moments. However, the

dx.doi.org/10.1021/ic401749q | *Inorg. Chem.* 2013, 52, 12599−12604

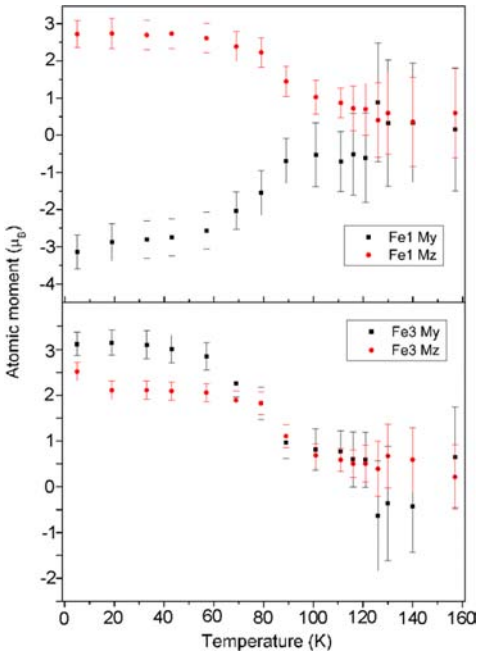

Figure 7. Temperature dependence of the M_y and M_z components of the Fe1 and Fe3 moments.

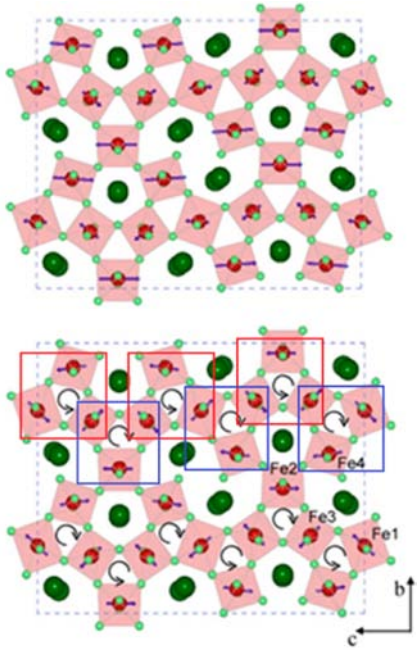

Figure 8. Refined magnetic structure of $K_3Fe_6F_{19}$ at 100 and 5 K (top and bottom, respectively). The red (blue) boxes highlight the triangular blocks of clockwise (counterclockwise) magnetic interactions forming stripes along the *c* direction.

performed refinement suggests that they are ferromagnetically ordered within the single chain, giving rise to a resultant moment in the *c* direction. However, the magnetic structure involving Fe1 and Fe3 is on the whole antiferromagnetic, the resultant moment of a chain being compensated by the one adjacent along *b*. The three-dimensional AFM nature of the global magnetic structure is preserved by the antiparallel stacking along *a* of the interactions in the *bc* plane. The stacking order is lost above 125 K, likely transforming the 3D order in a 2D one. By decreasing *T*, the triangular exchange interactions become dominant, driving the magnetic structure, through a spin rotation extending down to 60 K, to the final arrangement shown in Figure 8 for the 5 K refined data. Final convergence was achieved with $R(F^2)$ = 14% and χ^2 = 0.78. The corresponding Rietveld plot is shown in Figure 9, while the

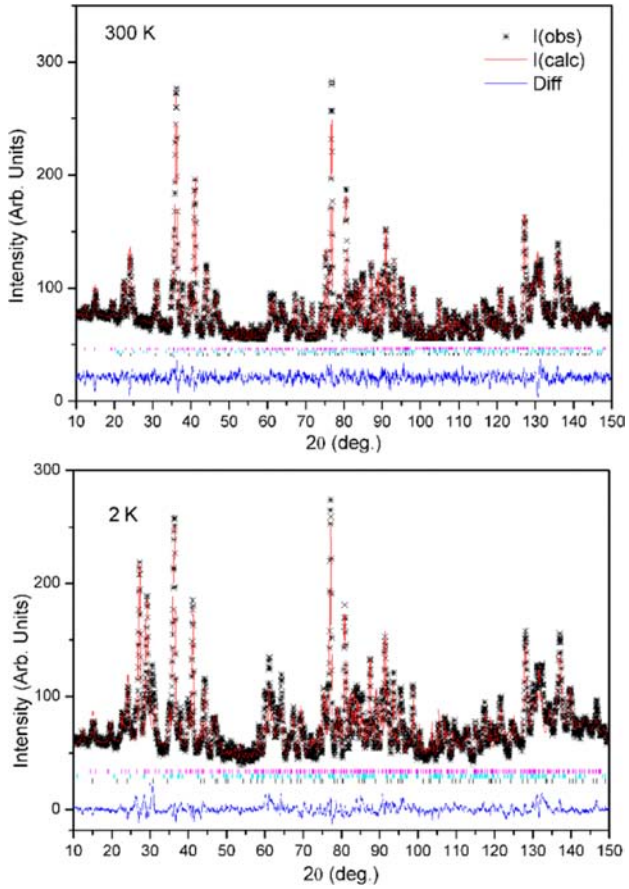

Figure 9. Rietveld plots of the neutron diffraction data collected at 300 and 2 K.

refined values of the moments are reported in Table S3, provided as Supporting Information. The spin ordering scheme is better visualized as stripes of triangular AFM interactions running along *c* (Figure 8). In a single triangular unit, the interaction is AFM, the spins being rotated by about 120°.

The stripes are formed by alternate sequences of triangles in which the spins are rotated in clock- and anticlockwise fashion. All the spin rotations are inverted in stripes adjacent along *b* as well as in the layers stacked along *a*, which are coupled antiferromagnetically. Neutron and X-ray powder diffraction data allowed the study of the cell volume as a function of temperature (Figure 10). The thermal behavior of the sample is fully reversible at both high and low temperature, and the compound results to being stable in the whole explored temperature range. No evidence of structural phase transitions is detected above RT up to 700 K, while, below RT, a variation of the thermal expansion coefficient is observed at 125 K, matching the AFM ordering transition.

■ CONCLUSIONS

$K_3Fe_6F_{19}$ is a TTB-related material showing peculiar structural features and complex magnetic behavior. The structure was

dx.doi.org/10.1021/ic401749q | *Inorg. Chem.* 2013, 52, 12599−12604

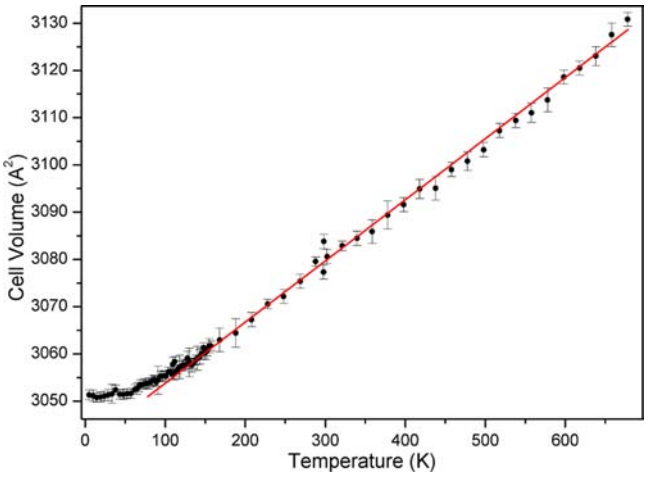

Figure 10. Cell volume as a function of temperature.

fully characterized by single-crystal X-ray diffraction. Structural building blocks, showing triangular and pentagonal cavities similar to those characterizing the TTB structure, are assembled in an unusual way by the presence of an additional octahedral FeF_6 unit. The perovskite cage, typical of $K_3Fe_5F_{15}$, is substituted by a larger S-shaped one, simultaneously occupied by two potassium ions. Like the classical TTB fluorides, $K_3Fe_6F_{19}$ shows charge order among the octahedrally coordinated Fe^{2+}/Fe^{3+} ions. Such a complex structure gives rise to peculiar magnetic behavior characterized by numerous critical effects. The interpretation of magnetic measurements performed on powder and single crystal samples was supported by neutron diffraction data analysis, allowing the determination of the magnetic structure of the system and of its evolution in temperature. Several magnetic transitions are observed: the first one, not revealed by neutron diffraction but observed as a weak effect in the magnetization measurements at 250 K, is likely related to the onset of short-range magnetic interactions. Long-range magnetic ordering takes place at lower temperature (125 K) and, in agreement with neutron diffraction, involves mostly one-half of the iron atoms, which align antiparallelly along the *c* direction; accordingly, an AFM signal is revealed at this temperature by the $M(T)$ curves performed on an oriented single crystal just when the field is applied along *c*. By decreasing *T*, the triangular exchange interactions become dominant, driving the magnetic structure, through a spin rotation that extends down to 60 K. Below 80 K, the remaining iron atoms suddenly increase their moments (with nonzero *b* and *c* components), and the complete order takes place below 60 K, where all the atomic moments become comparable in modulus. The spin ordering scheme can be visualized as stripes, running along *c*, formed by alternate triangular sequences of spins alternately rotated in clock- and anticlockwise fashion. While the $M(T)$ curves performed on an oriented single crystal with the field applied along *b* revealed an AFM signal at 80 K, powder measurements show the dominant magnetic effect at both 80 or 60 K, depending on the heating/cooling procedure and on the applied field. It is interesting to note that a magnetic field applied on heating along *b* forces the 3D order at higher temperatures, giving rise to a ferrimagnetic resultant that disappears at 250 K, that is, the onset temperature of short-range interactions.

■ ASSOCIATED CONTENT

Supporting Information

Complete crystallographic data are provided in the Supporting Information. This material is available free of charge via the Internet at http://pubs.acs.org.

■ AUTHOR INFORMATION

Corresponding Author

*E-mail: francesco.mezzadri@unipr.it.

Present Address

[⊥]IMEM-CNR, Area delle Scienze 37/A, 43124 Parma, Italy.

Notes

The authors declare no competing financial interests.

■ ACKNOWLEDGMENTS

The authors wish to acknowledge the Institute Laue-Langevin (Grenoble, France) for providing technical and financial support. F.M. is grateful to Roberta Magnani for help in sample preparation. The authors are also grateful to Fondazione Cariparma for financial support.

■ REFERENCES

(1) De Pape, R. *C. R. Acad. Sci.* **1965**, *260*, 4527−4530.
(2) Ravez, J.; Abrahams, S. C.; De Pape, R. *J. Appl. Phys.* **1989**, *65*, 3987−3990.
(3) Ravez, J.; Abrahams, S. C.; Mercier, A. M.; Rabardel, L.; De Pape, R. *J. Appl. Phys.* **1990**, *67*, 2681−2683.
(4) Mezzadri, F.; Calestani, G.; Pernechele, C.; Solzi, M.; Spina, G.; Cianchi, L.; Del Giallo, F.; Lantieri, M.; Buzzi, M.; Gilioli, E. *Phys. Rev. B* **2011**, *84*, 104418.
(5) Calage, Y.; Abrahams, S. C.; Ravez, J.; de Pape, R. *J. Appl. Phys.* **1990**, *67*, 430−433.
(6) Banks, E.; Nakajima, S.; Williams, G. J. B. *Acta Crystallogr., Sect. B* **1979**, *35*, 46−49.
(7) Mezzadri, F.; Fabbrici, S.; Montanari, E.; Righi, L.; Calestani, G.; Gilioli, E.; Bolzoni, F.; Migliori, A. *Phys. Rev. B* **2008**, *78*, 064111.
(8) Hemon, A.; Le Bail, A.; Courbion, G. *Eur. J. Solid State Inorg. Chem.* **1993**, *30*, 415−426.
(9) Hardy, A. M.; Hardy, A.; Ferey, G. *Acta Crystallogr., Sect. B* **1973**, *29*, 1654−1658.
(10) Kim, S. W.; Kim, S.-H.; Halasyamani, P. S.; Green, M. A.; Bhatti, K. P.; Leighton, C.; Das, H.; Fennie, C. J. *Chem. Sci.* **2012**, *3*, 741−751.
(11) Burla, M. C.; Caliandro, R.; Camalli, M.; Carrozzini, B.; Cascarano, G. L.; De Caro, L.; Giacovazzo, C.; Polidori, G.; Spagna, R. *J. Appl. Crystallogr.* **2005**, *38*, 381−388.
(12) Sheldrick, G. M. *SHELXL93: Program for the Crystal Structure Refinement*; University of Göttingen: Göttingen, Germany, 1993.
(13) Larson, A. C.; Von Dreele, R. B. *General Structure Analysis System (GSAS)*; Report LAUR 86-748; Los Alamos National Laboratory: Los Alamos, NM, 2000.
(14) Toby, H. B. *J. Appl. Crystallogr.* **2001**, *34*, 210−213.
(15) Heger, G.; Geller, R. *Phys. Status Solidi* **1972**, *53*, 227−234.
(16) Desert, A.; Bulou, A.; Leblanc, M.; Nouet, J. *J. Phys.: Condens. Matter* **1998**, *10*, 9067−9079.